Title	Focusing Characteristics of High Energy Density Beam
Author(s)	Arata, Yoshiaki; Ishimura, Tsutomu; Miyamoto, Isamu
Citation	Transactions of JWRI. 1973, 2(1), p. 1-6
Version Type	VoR
URL	https://doi.org/10.18910/8795
rights	
Note	

Focusing Characteristics of High Energy Density Beam[†]

Yoshiaki ARATA*, Tsutomu ISHIMURA** and Isamu MIYAMOTO***

Abstract

Mathematical formulations which give power density of a focused beam are proposed. The calculated values are compared with experimental data obtained from CO_2 laser and electron beams. It is shown that both are considerably coincidental.

1. Introduction

In the heat processing such as welding, cutting and drilling, phenomena occurring in the process differ according to energy density and its distribution of the heat source used, thereby affecting the quality of the processed goods. Laser and electron beams, which can be well concentrated, producing considerably higher energy density than conventional heat source, have not only improved the quality but even enable the processing which has been impossible. However, knowledge of the energy densities and distributions of the sources such as laser and electron beams, which are concentrated by a lens, is not sufficient, in spite of their importance, because of the difficulty of experimental and theoretical treatments.

In general, as the beam has a certain divergency which varies with many factors including beam species, quality, energy density and so on, it is almost impossible to propose the precise energy density of the focused beam. In this paper the energy density distribution is proposed theoretically by assuming the beam divergence to be uniform in all portions for simplicity, and is compared with the experimental data obtained from laser and electron beams.

2. Energy Density Distribution of Focused Beam

In order to calculate the energy distribution of the focused beam the following two assumptions are introduced:

1) The beam radiated from a point diverges in a cone like shape of which axis is in the radiated direction.
2) Its beam energy density in the plan perpendicular to the axis is given by a Gaussian curve.

Then the beam power $f(x, y, z)$ in the xy plane at (x, y, z) due to the limited beam $q \cdot ds$ radiated from the origin in the direction to the z axis is given by

$$f(x, y, z) = \frac{q}{2\pi\sigma_0^2 z^2} \, exp\left(-\frac{x^2+y^2}{2\sigma_0^2 z^2}\right), \quad \text{----------- (1)}$$

where σ_0 is the standard deviation of the Gaussian curve at $z=1$.

Here the power distribution of the beam around the origin is proposed under condition the beam $q = q(X, Y)$ in the $z=Z$ plane is directed toward the origin as shown in **Fig. 1**. The beam $q \cdot dx \cdot dy$ from a small area $dx \cdot dy$ at point $S(X, Y)$ provides the beam power density in the plane perpendicular to the z axis at point $A(x, y, z)$ given by the following equation:

$$f(x, y, z; X, Y) = \frac{q \, dx \, dy}{2\pi\sigma_0^2 l^2} \, exp\left(-\frac{m^2}{2\sigma_0^2 l^2}\right) \, cos\beta. \text{ --(2)}$$

Where

$$l = \overline{SB} = \frac{X^2+Y^2+Z^2-(xX+yY+zZ)}{\sqrt{X^2+Y^2+Z^2}},$$

$$m = \overline{AB} = \left[\frac{(x^2+y^2+z^2)(X^2+Y^2+Z^2)-(xY+yX+zZ)^2}{X^2+Y^2+Z^2}\right]^{\frac{1}{2}} \quad (3)$$

and

$$cos\beta = \frac{Z-z}{\sqrt{(X-x)^2+(Y-y)^2+(Z-z)^2}}.$$

(β represents the angle between $\overline{AS}$ and the z axis). Putting $x = rcos\theta$, $y = rsin\theta$, $X = Rcos\Theta$ and $Y = Rsin\Theta$, l, m and $cos\beta$ may be written as follows;

$$l = \frac{R^2+Z^2-(rRcos\varphi+zZ)}{\sqrt{R^2+Z^2}},$$

$$m = \left[\frac{(r^2+z^2)(R^2+Z^2)-(rR\cos\varphi+zZ)^2}{R^2+Z^2} \right]^{\frac{1}{2}} \quad \text{---- (4)}$$

and

$$\cos\beta = \frac{Z-r}{\sqrt{R^2+Z^2-2rR\cos\varphi-2zZ+r^2+z^2}} ,$$

where $\varphi = \theta - \Theta$.

When the beam power is constant in a circlar region of radius R_0;

$$q(R, \Theta) = \left\{ \begin{matrix} q_0, & R \leq R_0 \\ 0, & R > R_0 \end{matrix} \right\} , \quad \text{---------------------- (5)}$$

and is focused through a lens of the focal length $Z = D_F$, the beam power in a plane vertical to the z axis at location $A(x, y, z)$ is given by

$$w_b(x, y, z) = \int_0^{R_0}\int_0^{2\pi} f(x, y, z; R, \Theta) R\, dR\, d\Theta . \quad (6)$$

Now the following assumptions are introduced;
1) Radius of the beam source in $z = D_F$ plane is sufficiently smaller than the focal length; $R_0 \ll D_F$.
2) The values r and z treated here are limited to a sufficiently small region in comparison with source radius R_0 and focal length D_F, respectively, $r \ll R_0$ and $z \ll D_F$.
Then it becomes

$$l^2 \approx z^2 ,$$

$$m^2 \approx \frac{r^2 D_F^2 + z^2 R^2 - 2rzRD_F\cos\varphi}{D_F^2} \quad \text{---------------- (7)}$$
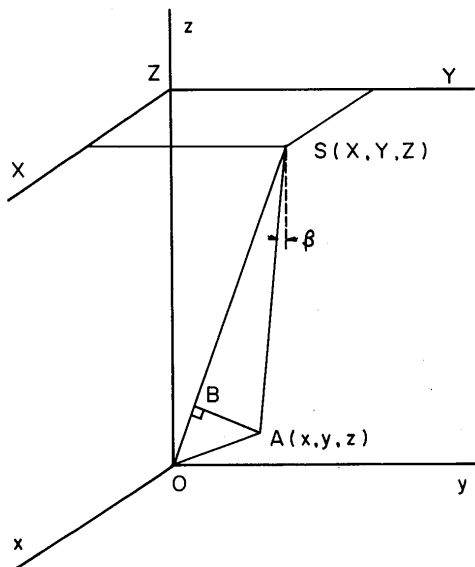
and

Fig. 1. Beam radiated from point $S(X, Y, Z)$.

$$w_b(r, \theta, z) = \frac{q_0}{2\pi\sigma_0^2 D_F^2}$$

$$\times \int_0^{R_0}\int_0^{2\pi} \exp\left(-\frac{r^2 D_F^2 + z^2 R^2 - 2rzRD_F\cos\varphi}{2\sigma_0^2 D_F^4}\right)$$

$$\times RdRd\varphi = \frac{q}{\sigma^2}\int_0^{R_0} \exp\left(-\frac{r^2 D_F^2 + z^2 R^2}{2\sigma_0^2 D_F^4}\right)$$

$$\times I_0\left(\frac{rzR}{\sigma^2 D_F^3}\right) RdR \quad \text{-------------------- (8)}$$

where $I_0(a)$ represents the modified Bessel function of the first kind of order zero. Putting

$$Q = \pi R_0^2 q_0 ,$$
$$\sigma_F = \sigma_0 D_F, \quad \text{------------------------------------- (9)}$$
$$r^* = r/\sigma$$

and

$$z^{*\prime} = \frac{Z}{\sigma_F} \cdot \frac{R}{D_F} ,$$

it may be written

$$w_b(r^*, z^*) = \frac{Q}{2\pi\sigma_F^2} \cdot \frac{2}{z^{*2}} \int_0^{z^*} exp\left(-\frac{z^{*\prime2}+r^{*2}}{2}\right)$$

$$\times I_0(z^{*\prime} r^*) z^{*\prime} dz^{*\prime} \quad \text{----,----------------- (10)}$$

where $z^* = (z/\sigma_F)(R_0/D_F) = z/\sigma_F \tan\theta_b$ and $2\theta_b$ represents convergence angle. At focal point, $r^* = z^* = 0$, it becomes

$$w_b(0, 0) = \frac{Q}{2\pi\sigma_F} \equiv w_{bm} \quad \text{--------------------------- (11)}$$

Normalizing the value of $w_b(r^*, z^*)$ by that of focal point w_{bm},

$$w_b^*(r^*, z^*) = \frac{2}{z^{*2}} \int_0^{z^*} exp\left(-\frac{z^{*\prime2}+r^{*2}}{2}\right) \cdot I_0(z^{*\prime}r^*)$$

$$\times z^{*\prime} dz^{*\prime} \quad \text{-------------------------------- (12)}$$

Writing $I_0(a)$ in the form

$$I_0(a) = \sum_{n=0}^{\infty} \frac{a^{2n}}{2^{2n}(n!)^2} \quad \text{-------------------------------- (13)}$$

Eq (12) becomes

$$w_b^*(r^*, z^*) = \frac{2}{z^{*2}} \int_0^{z^*} exp\left(-\frac{z^{*\prime2}+r^{*2}}{2}\right)$$

$$\times \sum_{n=0}^{\infty} \frac{z^{*\prime2n+1} r^{*2n}}{2^{2n}(n!)^2} dz^{*\prime} \quad \text{------------------ (14)}$$

As the results of the partial integration of Eq (14),

$$w_b{}^*(r^*, z^*) = \frac{2}{z^{*2}} \left[1 - exp\left(-\frac{z^{*2} + r^{*2}}{2}\right) \right.$$

$$\left. \times \sum_{n=0}^{\infty} \sum_{m=0}^{n} \frac{1}{n!m!} \left(\frac{z^*}{2}\right)^{2m} \left(\frac{r^*}{2}\right)^{2n} \right] \quad \text{------(15)}$$

In special cases;
1) in the focal plane, $z^* = 0$,

$$w_b{}^*(r^*, 0) = exp\left(-\frac{r^{*2}}{2}\right) \quad \text{------------------------(16)}$$

2) on the beam axis, $r^* = 0$,

$$w_b{}^*(0, z^*) = \frac{2}{z^{*2}} \left[1 - exp\left(-\frac{z^{*2}}{2}\right)\right] \quad \text{-----------(17)}$$

In Figs. 2 and 3 nomalized beam power density in the planes perpendicular to the z axis and parallel to the z axis is plotted. On the beam axis the beam power density falls to e^{-1} of w_b (0, 0) at $z^* = 2.23$. This corresponds to $z = 2.23\sigma/\tan\theta_b$. Recently one of the authors named the length along the beam axis between w_b (0, 0)/e points above and below focal point as "beam active length", l_b given by

$$l_b = 4.46\frac{\sigma}{\tan\theta_b} \quad \text{------------------------------------(18)}$$

where $2\theta_b$ represents the convergence angle of the beam toward the focal point.

3. Comparison with Experimental Results

3.1 Experimental Setup and Method

Two kinds of beams—laser and electron beams were used in order to check the theoretically analysed results described in the last section. One beam was obtained from the CO_2 laser which consisted of a water-cooled discharge tube 74 mm i. d., 12 m long, placed between gold evaporated plane and 29.2 m radius curvature mirrors (Ref. 1). The multimode laser power with a wavelength 10.6 μ was coupled out from the cavity through 15 mm diam hole at the center of the plane mirror. The coupled out beam was focused through a concave spherical mirror 2.0 m away from the laser head. Another beam 'was produced from electron beam apparatus, 150 KV-40 mA type (Hamilton Standard Division).

The test piece put on the slant, which moved horizontally at a constant speed v_b as shown in **Fig. 4**, was irradiated by the beam and the width of the fused bead or groove was measured. The contour of the width represents the equi-power line if there is no heat
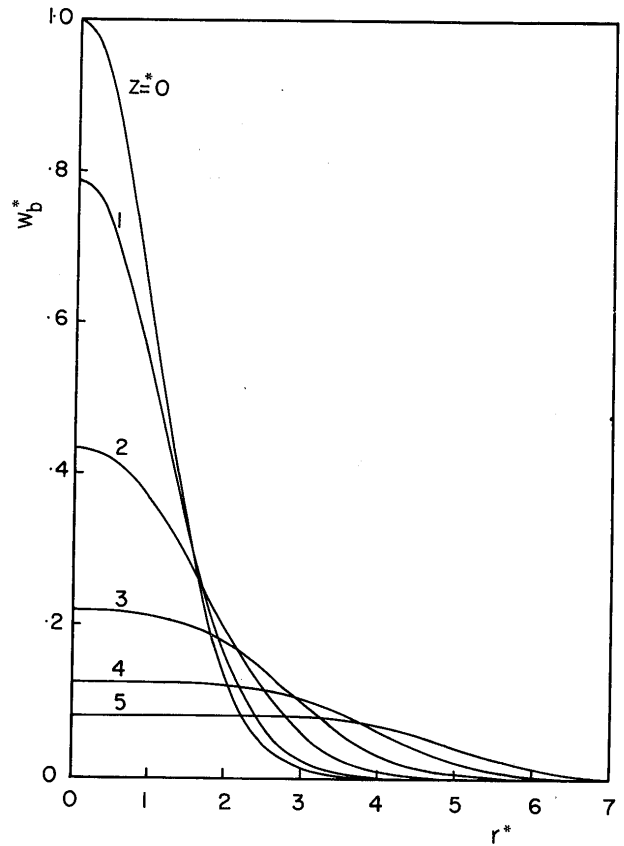
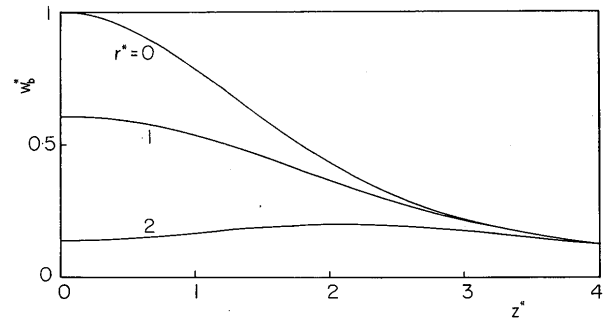Fig. 2. Relation between $w_b{}^*$ and r^* for various z^*.
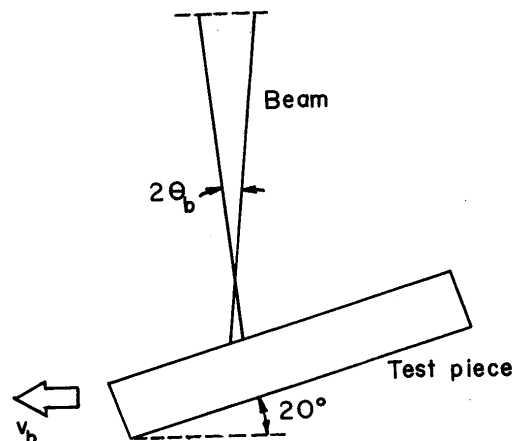
Fig. 3. Relation between $w_b{}^*$ and z^* for various r^*.

Fig. 4. Schematic diagram of experimental setup.

Table 1. Composition of SUS316L steel (%).

C	Si	Mn	P	S	Ni	Cr	Mo
0.03	1.0	2.0	0.04	0.03	12—16	16—18	2—3

conduction. Here the materials with low thermal conductivity—acryl for laser beam and austenitic SUS316L steel were used to minimize the effect of the thermal conduction. The composition of SUS316L steel was shown in **Table 1**.

3.2 CO_2 Laser Beam

The multimode CO_2 laser beam coupled out from the hole of diameter 15 mm was focused by means of a concave spherical mirror of focal length $D_F=155$ mm at distance about 2 m from the coupling hole in the same way as mentioned in Ref. 1; in this way the incident beam to the mirror was off-axial, but the effect of the astigmatism could be disregarded by making the incident angle small.   Energy density distribution in the plane vertical to the beam axis at the focal point was measured and it was found that the profile coincided quite well with the   Gaussian curve of standard   deviation $\sigma_F=0.177$ mm $(\sigma_0=1.14\times10^{-3})$ (Ref. 1).

Assuming that for the beam reflected from the spherical mirror Eq. (1) is valid and the beam power density is uniform in the circular region of the effective radius R_0, for simplicity, the beam source assumed in section **2** may be regarded to be at the mirror surface. In order to obtain the effective source radius R_0, a film was placed at mirror surface and irradiated by the laser beam for a short time.   The radius of the scoached area of the film was about 9.8 mm. Then r^* and z^* are given as follows:

$$r^*=\frac{r}{\sigma_F}=5.65\ r$$

$$z^*=\frac{z}{\sigma_F}\frac{R_0}{D_F}=0.36\ z\ .$$

As the moving slant test piece shown in **Fig. 4** continuously irradiated by the laser beam, wedge-shaped deep groove was formed, and width of the groove at its surface was measured. In **Fig. 5** the experimental data of the half width r are plotted in the cases of $v=2$ cm/sec, 5 cm/sec and 6 cm/sec. As values r in mirror side and the opposite side were almost symmetric with respect to the focal point,   the mean value of both was plotted.   In this figure solid lines show theoretical value and agree well with the experimental data. Since the laser power level is 85W, energy density w_{bm} at the focal point, $r^*=z^*=0$, is about 430 W/mm^2. For example, 4.3 W/mm^2 is ob-
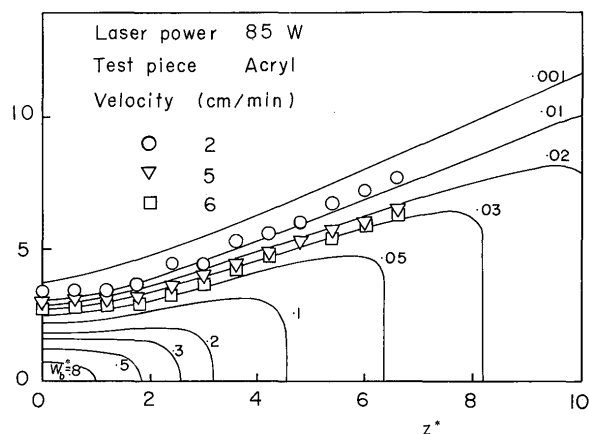

Fig. 5. A comparison of theoretical values with experimental data obtained from laser beam.

tained at $w_b^*=0.01$. The thermal conductivity of acryl is exceedingly small, of the order 10^{-4} cal/sec °C cm so that energy density at the groove edge divided by the velocity of the test piece v_b may be regarded to be constant. It corresponds to 217 (W/cm^2) (cm/sec) in both cases of $v_b=2$ cm/sec and 6 cm/sec as shown in **Fig. 5**.

3.3 Electron Beam

It has been experimentally made clear by A. Sanderson that energy density distribution can be approximated by a Gaussian curve (Ref. 2). According to his data standard deviation of the Gaussian curve σ_F is 0.06 ~ 0.07 mm when accelerating voltage $V_b=$ 30 KV and beam current $I_b=10$ mA, and here 0.06 mm was adopted expediently.

A series of experimens was performed under various conditions and the bead width was measured (R,ef. 3).   In **Fig. 6** the bead half width is plotted against the distance from the focal lens for SUS316L steel, for example.   The contour of the bead was not symmetric with respect to the focal point; the width at lens side was somewhat smaller than that at the opposite side.
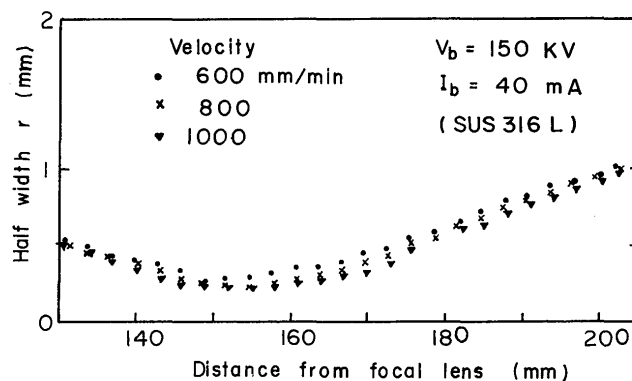

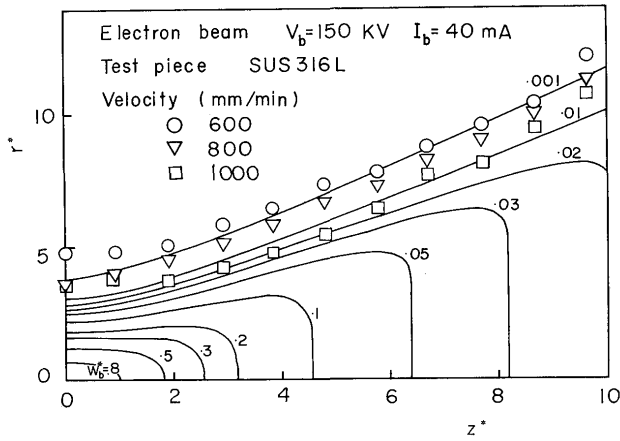Fig. 6. Half beam width plotted against the distance from a focal lens.

Fig. 7. A comparison of theoretical values with experimental data obtained from electron beam.

Fig. 8. The values of r_0 and σ_0 plotted against focal length.

In **Fig. 7** the data are compared with the equi-power lines in r^*-z^* co-ordinates obtained from theoretical analysis. When data were converted into non-dimensional values, r^* and z^*, $\sigma_F = 0.06$ mm and $\tan\theta_b$ $=1/52$ were used. The convergency angle θ_b was proposed from the inclination of the linear part of the curve imagined from the data, where the beam source was assumed to locate at the center of the lens in the same manner as the laser beam. For the half bead width the average value of the lens side and opposite one was adopted. According to $\tan\theta_b = 1/52$, the effective radius of the beam source R_0 became about 3 mm. The expperimental data are a little bigger than the theoletical value around the focal point, but it can be said that both are considerably coincidental. This may be because electron velocity is not constant so that the beam does not converge toward a point. As the energy density at the focal point, $r^*=z^*=0$, w_{bm} $=I_b \cdot V_b/2\pi\sigma_F^2=2.56\times10^5$ W/mm^2, energy density at $w_b^*=0.001$, for example, corresponds to 2.65×10^2 W/mm^2.

The standard deviation, which represents the measure of the divergency of the electron beam, is affected by various factors. Here the effect of the focal length and the pressure in the chamber on the standard deviation is discussed, compared with the case of focal length 156 mm, in which σ_F equals 0.06 mm.

By controlling the current of lens coil the focal length D_F was varied. In **Fig. 8** half bead width at focal point r_0 is plotted for each focal length 0.22 mm, 0.23 mm and 0.27 mm. Neglecting the effect of the heat conduction, each point has the same energy density. The standard deviation of the Gaussian curve, which represents the energy density distribution,
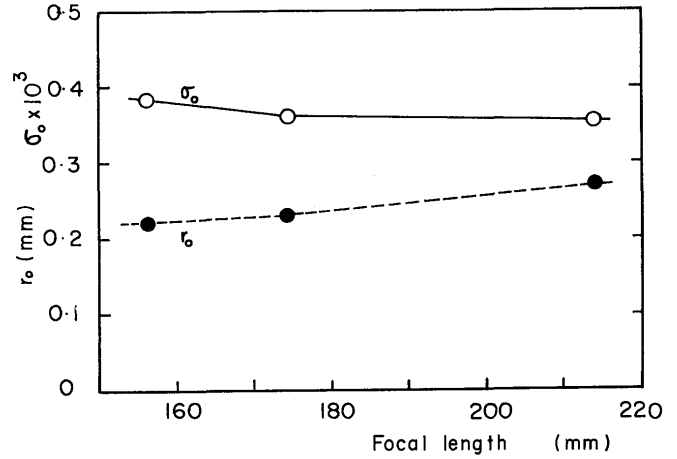
is equal to 0.06 mm as already mentioned. Thus the energy density at $r_0=0.22$ mm is given by

$$w_b \left(\frac{0.22}{\sigma_F}, 0\right) = w_{bm}\, exp\left(-\frac{r_0^2}{2\sigma_F^2}\right).$$

Therefore the standard deviations σ_1 and σ_2 in case of $D_F =174$ mm and 214 mm are respectively given by

$$w_{b_1} \left(\frac{0.22}{\sigma_{F1}}, 0\right) = w_{b_2}\left(\frac{0.27}{\sigma_{F2}}, 0\right) = w_{b_1}\left(\frac{0.22}{\sigma_F}, 0\right). \quad\text{-----} \quad (19)$$

Eq (19) provides $\sigma_{F1}=0.063$ and $\sigma_{F2}=0.076$ mm. Dividing each σ_F by the focal length, the standard deviation per unit length σ_0 is obtained, and is plotted in **Fig. 8.**

As the figure shows, there is such a tendency that σ_0 decreases a little with increase of the focal length. But the decrease is very small, so σ_0 can be regarded as constant. This result does not contradict the assumption described in section **2.**

The pressure in the chamber is usually maintained 10^{-4} torr order or less, and it is considered that as the gas pressure increases σ_0 varies because of scattering by the gas particles and interaction between electrons and plasma produced by the collision of the electrons with the gas particles. Assuming that there is a beam spread with the appearance of Gaussian distribution and there is no energy loss even if there are the scattering and the interaction, the standard deviation for each case can be calculated based on the experimental data having different chamber pressures.

Table 2 shows the data of half bead width at focal point and the values of standard deviation σ_0. When the pressure p increases slightly from 5×10^{-4} torr to 3×10^{-2} torr, shows a decrease of about 20 %, which is

Table 2. The values of σ_0 for different pressure ($D_F = 214$ mm).

Pressure (torr)	5×10^{-4}	3×10^{-2}	1×10^{-1}
r_0 (mm)	0.23	0.22	0.27
σ_0	3.55×10^{-4}	2.95×10^{-4}	2.0×10^{-3}

supposed to be caused by the lens effect of plasma (Ref. 4) produced by the beam collision.

From the figure it is seen that the energy density at the focal point has increased by about 1.5 times that of 5×10^{-4} torr.   In case of 1×10^{-1} torr, the beam is remarkably spread by the scatter, and energy density shows a decrease of about 3 % that of 5×10^{-4} torr.

References

1) Y. Arata and I. Miyamoto: "Some Fundamental Properties of High Power Laser Beam as a Heat Source—Beam Focusing Character-istics of CO_2 Laser—", Trans. Japan Welding Society, Vol. 3, No. 1 (1972).

2) A. Sanderson: "Electron Beam Delineation and Penetration", British W. J., Oct. 1968.

3) Y. Arata, H. Nagai and T. Hattori: "The Shape Decision of High Energy Density Beam", To be published.

4) Y. Arata and M. Tomie: "Non-vacuum Electron Beam (I)", Tech. Rept. Osaka Univ. Vol. 17, No. 773 (1967).

5) Y. Arata: "Characteristics of the Electron Beam Heat Soorce and View of the Development on Its Welding Technology", J. Japan Welding Society, Vol. 41 (1972) No. 11.